PROCEEDINGS OF SCIENCE

The Silicon Vertex Detector of the Belle II Experiment

H. Aihara[o], T. Aziz[g], S. Bacher[s], S. Bahinipati[d], E. Barberio[a], Ti. Baroncelli[a], To. Baroncelli[a], A. K. Basith[e], G. Batignani[h,i], A. Bauer[b], P. K. Behera[e], V. Bertacchi[h,i], S. Bettarini[h,i], B. Bhuyan[f], T. Bilka[c], F. Bosi[i], L. Bosisio[j,k], A. Bozek[s], F. Buchsteiner[b], G. Caria[a], G. Casarosa[h,i], M. Ceccanti[i], D. Červenkov[c], T. Czank[n], N. Dash[d], M. De Nuccio[h,i], Z. Doležal[c], F. Forti[h,i], M. Friedl[b], B. Gobbo[k], J. A. M. Grimaldo[o], K. Hara[p], T. Higuchi[♯l], C. Irmler[b], A. Ishikawa[n], H. B. Jeon[q], C. Joo[l], M. Kaleta[s], J. Kandra[c], K. H. Kang[q], P. Kodyš[c], T. Kohriki[p], I. Komarov[k], M. Kumar[u], R. Kumar[t], P. Kvasnička[c], C. La Licata[j,k], K. Lalwani[u], L. Lanceri[j,k], J. Y. Lee[r], S. C. Lee[q], Y. Li[v], J. Libby[e], T. Lueck[h,i], P. Mammini[i], A. Martini[h,i], S. N. Mayekar[g], G. B. Mohanty[g], T. Morii[l], K. R. Nakamura[p], Z. Natkaniec[s], Y. Onuki[o], W. Ostrowicz[s], A. Paladino[l], E. Paoloni[h,i], H. Park[q], K. Prasanth[g], A. Profeti[i], K. K. Rao[g], I. Rashevskaya[k,♯], P. K. Resmi[e], G. Rizzo[h,i], M. Rozanska[s], D. Sahoo[g], J. Sasaki[o], N. Sato[p], S. Schultschik[b], C. Schwanda[b], J. Stypula[s], J. Suzuki[p], S. Tanaka[p], H. Tanigawa[o], G. N. Taylor[a], R. Thalmeier[b], T. Tsuboyama[p], P. Urquijo[a], L. Vitale[j,k], K. Wan[o], M. Watanabe[m,♭], S. Watanuki[n], I. J. Watson[o], J. Webb[a], J. Wiechczynski[s], S. Williams[a], H. Yin[b], L. Zani[h,i] [Belle II SVD Collaboration]

[a] *School of Physics, University of Melbourne, Melbourne, Victoria 3010, Australia*
[b] *Institute of High Energy Physics, Austrian Academy of Sciences, 1050 Vienna, Austria*
[c] *Faculty of Mathematics and Physics, Charles University, 121 16 Prague, Czech Republic*
[d] *Indian Institute of Technology Bhubaneswar, Satya Nagar, India*
[e] *Indian Institute of Technology Madras, Chennai 600036, India*
[f] *Indian Institute of Technology Guwahati, Assam 781039, India*
[g] *Tata Institute of Fundamental Research, Mumbai 400005, India*
[h] *Dipartimento di Fisica, Università di Pisa, I-56127 Pisa, Italy*
[i] *INFN Sezione di Pisa, I-56127 Pisa, Italy*
[j] *Dipartimento di Fisica, Università di Trieste, I-34127 Trieste, Italy*
[k] *INFN Sezione di Trieste, I-34127 Trieste, Italy*
[l] *Kavli Institute for the Physics and Mathematics of the Universe (WPI), University of Tokyo, Kashiwa 277-8583, Japan*
[m] *Department of Physics, Niigata University, Niigata 950-2181, Japan*
[n] *Department of Physics, Tohoku University, Sendai 980-8578, Japan*
[o] *Department of Physics, University of Tokyo, Tokyo 113-0033, Japan*
[p] *High Energy Accelerator Research Organization (KEK), Tsukuba 305-0801, Japan*
[q] *Department of Physics, Kyungpook National University, Daegu 702-701, Korea*
[r] *Department of Physics and Astronomy, Seoul National University, Seoul 151-742, Korea*
[s] *H. Niewodniczanski Institute of Nuclear Physics, Krakow 31-342, Poland*
[t] *Punjab Agricultural University, Ludhiana 141004, India*
[u] *Malaviya National Institute of Technology Jaipur, Jaipur 302017, India*
[v] *Peking University, Department of Technical Physics, Beijing 100871, China*
♯ *presently at TIFPA - INFN, I-38123 Trento, Italy*
♭ *presently at Nippon Dental University, Niigata 951-8580, Japan*

PoS(VERTEX2018)024

The silicon vertex detector (SVD) for the Belle II experiment at the SuperKEKB accelerator in Japan is responsible for detecting particle's origins. It comprises four cylindrical layers with ladder-like double-sided silicon detector (DSSD) arrays on each layer. The ladders produced under a stringent quality control showed good mechanical tolerance with a DSSD distortion <300 μm and with an electrical efficiency $>99\%$. The SVD was commissioned with cosmic-ray events for two months. Cluster-finding efficiency was estimated in the commissioning to be $>98.5\%$. The commissioned SVD had been installed on the Belle II detector. The so-called "phase 3" of the experiment with the SVD will start in March 2019.

The 27th International Workshop on Vertex Detectors - VERTEX2018
22-26 October 2018
MGM Beach Resorts, Muttukadu, Chennai, India

*Speaker.

1. Introduction

Despite the great success of the Standard Model (SM) of particle physics, the SM is not a complete theory to explain all mysteries in the universe, and it is strongly believed that a new physics accountable for the mysteries exists beyond the SM. Aiming at a search for the new physics, we started high energy experiment Belle II in KEK, Japan, in April 2018 [1].

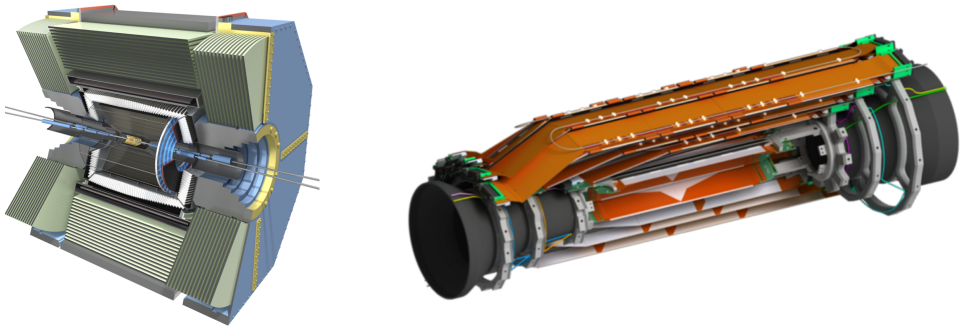

Figure 1: Sketches of the Belle II detector (left) and the SVD (right). The characteristic lantern shape is seen in the right sketch.

The SuperKEKB accelerator [2] is a circular collider of 7.0 GeV electrons to 4.0 GeV positions to deliver the B, D, τ, and other particle decays to the experiment, and the Belle II detector [3] sketched in Figure 1 (left) precisely measures the decay-particle properties with covering the e^+-e^- interaction region. The detector comprises seven sub-detectors: pixel detector (PXD) and silicon vertex detector (SVD) for detecting the particle's origin, central drift chamber for particle tracking and dE/dx measurement, aerogel ring-image Cherenkov counters and time-of-propagation counters for particle identification, electromagnetic calorimeter for particle energy measurement, and K_L^0-μ detector for K_L^0 and $\mu^\pm$ detection. The combination of the PXD and SVD (referred to as the vertex detector (VXD), hereafter) is estimated to detect a particle position having a transverse momentum of $p_\mathrm{T} = 2$ GeV/c with an impact parameter resolution of 15 μm.

The accelerator and detector were commissioned taking a phase-by-phase approach. In Phase 1 from February to June 2016, the accelerator was commissioned while the detector was out of the beam line to avoid possible large radiation dose on the detector from the accelerator under the commissioning. The e^+ and e^- beams were successfully stored in the SuperKEKB rings in Phase 1. In April 2017, the Belle II detector equipped with all the sub-detectors but the VXD was rolled in to the interaction region. Phase 2 was started in March 2018, and on April 26$^{\mathrm{th}}$, the first hadronic event of $e^+e^- \to q\bar{q}$ was confirmed with the Belle II detector, upon which the start of the Belle II experiment was claimed. The SuperKEKB accelerator had achieved a peak luminosity of 2.29×10^{33} cm^{-2}s^{-1}, and the Belle II detector has collected $\sim$454 pb^{-1} of data by the end of Phase 2 in July.

2. SVD Overview

A sketch of the SVD is shown in Figure 1 (right). The SVD consists of four cylindrical layers (layer 3 to 6) with their radii being 39, 80, 104, and 135 mm, respectively. The layers comprise 7, 10, 12, and 16 ladder-like arrays of double-sided silicon strip detectors (DSSDs), and each ladder

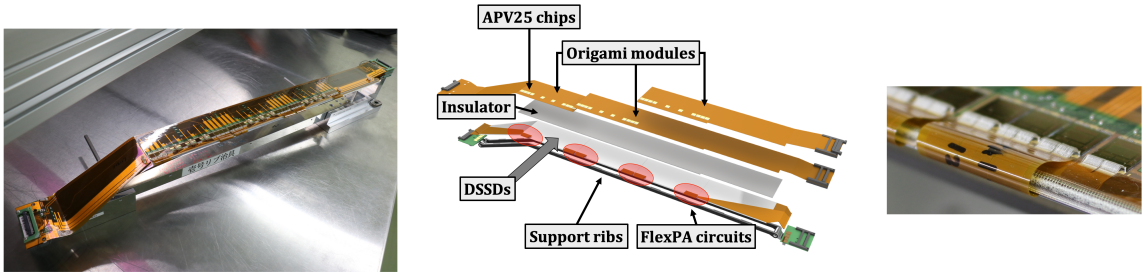

Figure 2: Photos of the assembled layer-6 ladder (left) and its anatomy (center), and the photo of the FlexPA circuit extracted from the top side and bent to the APV25 chips (right).

is composed of 2 to 5 DSSDs. The ladders are mounted on forward and backward end rings to form the cylindrical shape. In order to reduce the material budget in the forward region, the SVD has a characteristic lantern shape, and the layer 4 to 6 ladders are designed to have a slant structure in the forward region. The ladder is composed of ladder support ribs, DSSDs, thermal insulator, readout ASIC chips (APV25 chips), readout flexible printed circuit boards (Origami PCBs), and small PCB cards (Hybrid cards). The assembled layer-6 ladder and its anatomy are shown in Figure 2 (left and center, respectively). The components are mostly glued with epoxy adhesive. Three kinds of DSSDs are used in the SVD; the layer 3 ladder employs a small rectangular DSSD, while the layer 4 to 6 ladders employ a large rectangular DSSD for the barrel part and a trapezoidal DSSD for the slant part. The long strips are located on the p side along the beam axis, and the short strips are located on the n side with an orthogonal arrangement to the p strips. On the p and n sides, 768 and 768 strips are lined on the layer 3 DSSD, and 768 and 512 strips are lined on the layer 4 to 6 DSSDs. The p side of all DSSDs, but the layer 3, faces the beam pipe; the layer 3 DSSDs are oppositely arranged.

The SVD signals are read out by 1,748 APV25 chips [4], which were originally developed for the CMS experiment. The short shaping time (50 ns) and deep analog pipeline (192 cells) of the chip contribute to minimizing signal pile up and readout dead time. The strips are electrically connected to the APV25 chips by wire bonding and flexible fan-out circuits. Strip signals on the most forward and backward DSSDs are transmitted to the APV25 chips mounted on the Hybrid card attached to each ladder end. Strip signals on the other DSSDs are transmitted to the APV25 chips mounted on the Origami PCBs directly glued on the DSSD n side via a foam insulator. The scheme, coined "chip-on-sensor" concept, reduces the capacitive noise by minimizing the signal path length rather than transmitting the signals to the ladder ends as the legacy ladder designs. The p side signals on the layer 4 to 6 ladder DSSDs are once extracted to the DSSD outside with the FlexPA circuits, and transmitted to the APV25 chips also mounted on the Origami PCBs by bending the FlexPA circuit as shown in Figure 2 (right). The bent FlexPA circuit is glued on the Origami PCB. The bending scheme is called the "Origami" concept.

Figure 3 shows the data stream from the SVD to the readout PCs. The SVD signals are transmitted to 48 VME-9U sized FADC modules, each of which is equipped with the AD9212 analog-to-digital converter chips linked to the individual APV25 chip and the Altera Stratix IV

FPGA for the following digital data processing. The digitized data undergo five steps of processing: FIR filtering for compensating line signal distortions, signal extraction, pedestal subtraction, common mode correction, and zero suppression. After hit time finding in the processed data, the data are transmitted to common data-acquisition platform modules, named COPPER [5], along a homemade data-link protocol over optical fibers. The data in the COPPER modules are read out by nine readout PCs and sent to event building PCs.

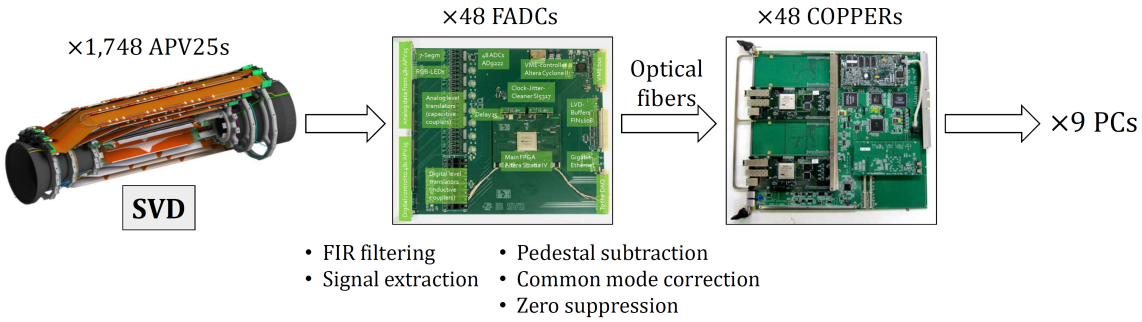

Figure 3: Illustration of the SVD data stream.

The APV25 chip dissipates 0.35 W heat once it is configured. All chips are thermally connected to a CO_2 cooling pipe via a piece of thermal-conductive silicon rubber (and an aluminum block as a heatsink for forward and backward chips), and cooled down by gas-liquid two-phase CO_2 with a temperature of -20 C°. The ladder temperatures are monitored by 248 sensors on 40 optical fibers inserted between the thermal insulator and Origami PCB for each ladder, and the end-ring temperatures are monitored by 64 NTC thermistors attached on the rings. The SVD volume is filled with nitrogen gas at room temperature. The nitrogen dew point is well below -30 C° to avoid dew condensation on the SVD. An interlock signal is issued when one of the monitors detects a faulty environment.

The instantaneous and integrated radiation doses on the VXD are monitored with 28 diamond sensors attached on the beam pipe and end rings. Diamond crystals work as an ionization chamber with an accurate dose measurement and proper responses to both fast and slow increases of the dose. The sensors have already been calibrated with β rays of strontium 90. A beam-abort signal is issued to the SuperKEKB accelerator when the monitor detects a radiation level exceeding a threshold.

3. SVD Ladder Assembly

Five institutes across the globe were responsible for assembly of forward and backward DSSD modules and layer 3 to 6 ladders, respectively: INFN Pisa (Italy), Melbourne University (Australia), TIFR (India), HEPHY (Austria), and Kavli IPMU (Japan).

Three essential items existed in the ladder-assembly procedure: DSSD alignment, component gluing, and wire bonding. The alignment tolerance of the DSSDs in each ladder was set to ± 300 μm to secure a sufficient space avoiding a touch of the fragile DSSD to any other components because the minimum proximity of a certain DSSD to the neighboring ladder component in the completed SVD was only 1 mm. For the precision sensor alignment, the DSSDs were handled

with tailored jigs having a machining precision of $\mathcal{O}(50\ \mu\mathrm{m})$ in the critical part. The DSSDs were initially aligned on the jigs with a coordinate measuring machine, and then chucked to the jig by vacuum. The alignment distortion in passing the sensors across two jigs was avoided by connecting the jigs with precision pins.

Since wire bonding on a FlexPA circuit demanded rigidly cured glue under the wire bonding pads as a foundation, glue underflow under the FlexPA circuit had to be avoided. Contrary glue overflow from the FlexPA edge also had to be avoided because it risked tainting the pads, which made the following wire bonding on the pads impossible. For these reasons, a gluing procedure ensuring the good glue spread was carefully developed. The procedure varied site by site. One site employed a 3D robot arm and compressed air supplier with controllable pressure to reproduce the amount and position of the dispensed glue on the FlexPA circuit; in the site, the glue viscosity was checked by drawing a check pattern on a plastic film every time before they used glue.

The DSSDs, FlexPA circuits, and APV25 chips are electrically connected by the ultrasonic wire bonding with $\phi = 25\ \mu$m aluminum wire. Parameters for the wire bonding machine were so tuned to provide a wire-bonding quality satisfying the following quality guideline: the bonding efficiency $\varepsilon > 99\%$, pull strength $f > 5$ gW, and $\sigma_f / f < 0.2$, where σ_f is the standard deviation of the f distribution. Failed bonds were periodically detected by microscopic and electrical inspections and timely repaired. More details on ladder assembly and mechanics can be found in Ref. [6].

Rather stringent internal reviews on the ladder-assembly procedure were introduced to secure reproducibility of good-quality ladders in the distributed sites with limited valuable ladder components. The sites used only a standardized, frozen, and documented ladder-assembly procedure that had already been signed off by the reviewers before ladder mass production. Any errors during the mass production were reported to the reviewers, and, as well as the procedure sign off, countermeasures for the errors were also reviewed after intensive tests on a mockup module and signed off before its embedding to the standard procedure. Manpower of the sites was also reviewed to secure the operator healthiness and ladder quality. By May 2018, all the sites completed the ladder mass production. All the completed ladders underwent mechanical survey of the DSSD alignment with a coordinate measuring machine and an electrical test of the DSSD response with a laser or β-ray illumination. The DSSD displacement below 300 μm and electrical defect fraction about 1% were achieved in all ladders. The ladders were transported to KEK in a shock-safe container and, after a careful incoming inspection with optical survey and electrical test, they were stored in desiccators there.

4. SVD Half-Shell Construction

The SVD cylinder can be vertically separated into two half shells. A pin hole is opened at every ladder slot on each end ring of the half shells to accept pins protruding from both ladder ends. Figure 4 (left) shows a ladder mounting operation to the end rings. The rotational angle of the two end rings, which are tentatively connected to a rotational rod, was set around the rod so that the rod and ladder slot under mounting came on the same horizontal plane. First, the ladder for mounting was picked up from the container with a ladder-mounting jig, and then, fixed on a horizontally sliding stage together with the jig. The ladder with the stage was slid toward the ladder slot and stopped right before the ladder touched to the end rings. Once the ladder pin

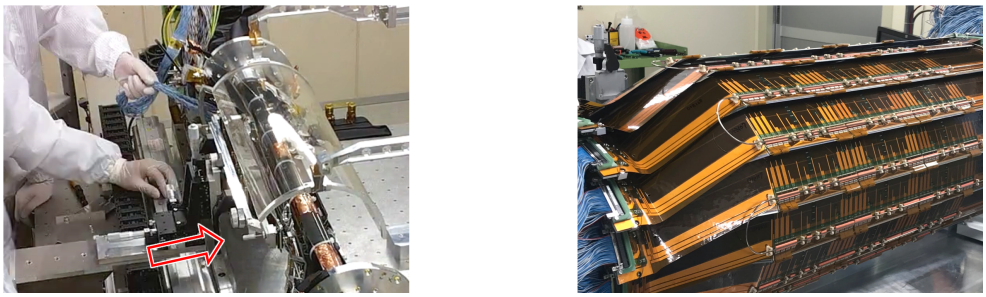

Figure 4: Photos of the ladder mounting operation (left) and completed half shell with all ladders and cooling pipes attached (right).

position was precisely adjusted to the pin hole position, the ladder was detached from the jig and inserted to the slot, and finally fixed to the end rings by screws. After each ladder was mounted on the rings, a quick electrical test was performed on the ladder itself and the neighbor ones to verify their integrity. Additional DSSD displacements from mounting were confirmed under control by a coordinate measuring system developed on the ladder mounting setup. No ladder components touched to others. After all ladders of the layer had been mounted on the half shell, the cooling pipe was attached on the shell, and the pipe was connected to a CO_2 supply. A dry box filled with dry air was built over the half shell for the following cooling test and electrical test of the full ladder, and then, the CO_2 supply was turned on. Good thermal contact between the pipe and chips was confirmed by monitoring the configured APV25 chips through an infrared camera. The electrical healthiness of the ladders in the completed layer was confirmed by analyzing calibration data from the ladders. The operation sequence was repeated for all the layers. The ladder mounting for both half shells had been completed by July 2018. A photo of one completed half shell is shown in Figure 4 (right). An overall electrical test of all the ladders on the fully dressed half shells was carried out, and no new electrical defects were detected in either half shell.

5. SVD Commissioning

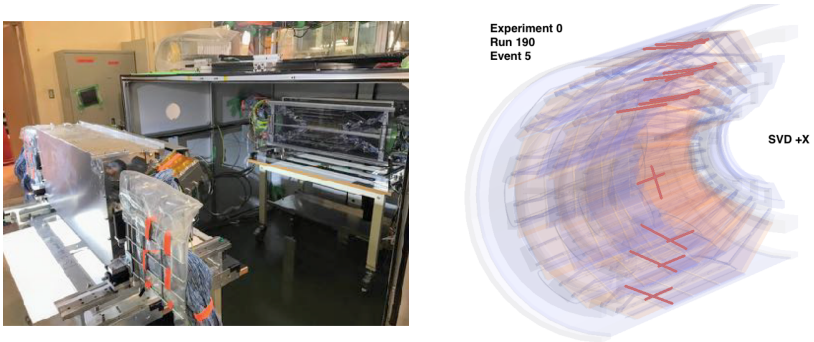

Figure 5: Photo of the half-shell commissioning setup with one half shell already in the dark box and the other one outside (left), and an early event display of a cosmic ray detected by the half shell (right).

The completed two half shells were commissioned from July to September 2018 in a full-scale test setup with cosmic rays. The shells were placed in a dark box (Figure 5, left), and connected to the 48 FADC modules. The COPPER modules and readout PCs for the experiment were used

to read out the FADC data while they were logically isolated from the central data acquisition system to avoid disturbing the data taking in Phase 2. Plastic scintillators were placed above and below each half shell to issue trigger signals for cosmic rays. The cooling pipes of the SVD were connected to a cooling plant developed as a part of the test setup. The SVD had collected 30×10^6 cosmic-ray events. The analysis results of the cosmic-ray data are described below.

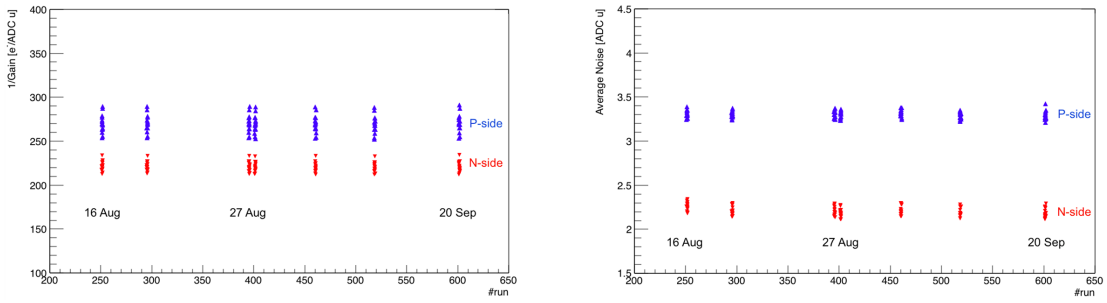

Figure 6: Calibration parameter trends for the gain (left) and noise (right) for selected 16 DSSDs in the two half shells monitored over the two-months commissioning. The parameters were stable over that period.

The calibration parameters gain and noise of both p and n sides of all the DSSDs were monitored over the two-months commissioning, and no significant trends in them were observed (Figure 6). The occupancies for each of p and n sides of all the DSSDs were also monitored during the commissioning, where the occupancy was defined as a fraction of strips with a signal-to-noise ratio larger than 5 to the total strips. The occupancies for cosmic-ray events were significantly higher than the random-trigger events, which meant the DSSD signals were properly dominated by cosmic-ray hits.

Cluster-energy distributions are shown in Figure 7. The distributions for the DSSDs horizontally arranged around the beam pipe peaked at a consistent number $\sim$80 keV to the energy deposition by a cosmic-ray approximated as a MIP almost perpendicularly entering into a 300 μm-thick silicon. The distribution peaks for slantingly and vertically arranged DSSDs tended to move larger side as expected because of the longer path length in the silicon. Peaks in the lowest energy region in the figure is considered coming from noise clusters. Figure 5 (right) shows an early event display of a cosmic ray detected by one half shell. Cluster-finding efficiencies of all DSSDs were found to be $>98.5\%$ and mostly $>99\%$, where the efficiency of a certain DSSD was defined by a number of associated clusters to the cosmic-ray intercept on the DSSD within a $\pm 500\mu$m range with subtracting a number of random-cluster contributions from the number of total clusters in the range.

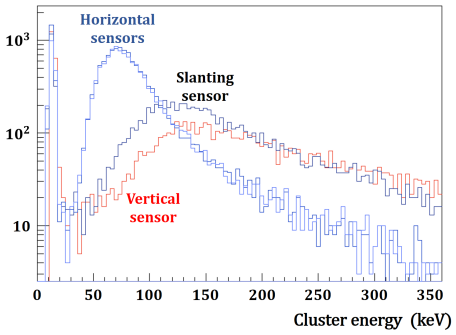

Figure 7: The cluster energy distributions for the DSSDs horizontally, slantingly, and vertically arranged around the beam pipe.

The commissioned SVD half shells were combined with the PXD by October 2018, and the VXD had been formed. The integrated system test on the VXD detected no new defects in it. The VXD has been installed to the Belle II detector in November 2018. The Belle II detector with all the sub-detectors installed is under the final commissioning before Phase 3 to start in March 2019.

6. Phase 2 Commissioning

Besides the ladder assembly, half-shell construction, and full-scale commissioning described in Sections 3 to 5, another VXD commissioning using a reduced-scale system, named BEAST (Figure 8), was carried out under the real beam environment in Phase 2 to confirm a safe beam-background environment toward the real VXD operation on the beam line in Phase 3. The BEAST detector was installed in the Belle II detector in November 2017, operated for the VXD commissioning throughout the Phase 2 period, and dismantled in September 2018 to make a space for the real VXD.

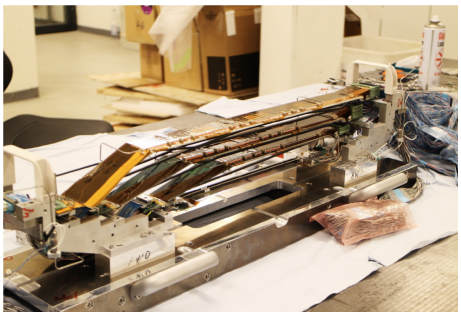

Figure 8: Photo of the BEAST detector, containing two PXD and four SVD ladders.

The occupancy limit of the SVD was set to $\lesssim$3% for an optimal tracking performance, and the radiation-dose limit on the SVD was set to $\lesssim$100 kGy for the 10-year Belle II operation (10 kGy/year) along conservatively estimated radiation hardnesses of the DSSD. According to Monte Carlo (MC) simulations of the beam background, the occupancy and annual radiation dose on layer-3 ladder under the full beam-current operation in Phase 3, were estimated to be $\sim$1% and $\sim$1 kGy/year, respectively. However, in analyzing the Phase 2 data, it was identified that the observed occupancy and MC-simulated occupancy for the corresponding beam conditions of Phase 2 were significantly incompatible, which would propagate in the worst case to scaling up the estimated background in Phase 3 by a factor 10-20. In this worst case scenario, pessimistically assuming the scaled-up estimation will be true, the scaled-up radiation dose will be still within the manageable level while the scaled-up occupancy will be beyond the operable level. While a source of the discrepancy between the observation and MC simulation is being investigated, an effort to mitigate the background will be made in the early Phase 3 period. The major occupancy sources are known to be Touschek background (Coulomb scattering of beam particles inside a beam bunch), beam-gas background (Bremsstrahlung and Coulomb scattering of a beam particle with residual gas in the beam pipe), and e^+-e^- collision. The first two are proportional to the electron beam current squared plus positron beam current squared, and the last one is proportional to an instantaneous luminosity. In the early Phase 3 stage when the accelerator will be operated with half beam currents of the full values used in the occupancy estimation, the occupancy will be a quarter of the worst case estimation and still below a manageable level to achieve good tracking performance. In the period, accelerator parameters and beam collimators will be tuned to mitigate the background.

The interlock systems were also tested in Phase 2. The radiation-monitoring and beam-abort system implemented with the diamond sensors were tested with setting the beam-abort threshold for a time-integrated dose over 10 ms to 5 μGy, which was lower than the nominal value, and increasing the beam currents eventually. The SuperKEKB beams were properly aborted by an abort request from the abort system when the time-integrated dose exceeded the threshold. A dose history stored in the radiation-monitoring electronics for the last one second before the abort was properly transmitted to an external device. The beam-abort thresholds for fast and slow aborts for the normal accelerator operation were set to 0.1 mGy/ms and 2 mGy/s, respectively; in Phase 2,

total 86 fast and 12 slow abort requests were issued. Finally, the interlock system for environmental monitors were also confirmed working properly. For some minor but real instances like a dew condensation close to the CO_2 transfer line due to a non-working vacuum pump causing insulation failure, the interlock system properly halted the SVD power supplies.

7. Summary

The Belle II experiment is searching for new physics beyond the SM. It has been kicked off in April 2018 with all the sub-detectors installed but the PXD and SVD. The PXD and SVD are the detectors for precisely locating particle origins. The SVD consists of four cylindrical layers with ladder-like DSSD arrays arranged on each layer. All the ladders had been produced with good mechanical and electrical qualities, and mounted on the end rings with no new additional electrical defects. The SVD was commissioned for two months with cosmic-ray events showing excellent performance. Calibration parameters gain and noise were confirmed stable over that period. The energy deposition on the DSSDs was consistent with expectation. The cluster finding efficiency was estimated to be $> 98.5\%$. According to background studies performed with Phase 2 data collected with a sector of SVD, the estimated radiation dose on the SVD, integrated over 10 years, is expected to be within a manageable level. Present estimation of the occupancy is expected to be beyond the level for an optimal tracking performance, but accelerator parameters and beam collimators still have to be tuned at the start of Phase 3 to mitigate machine background. The interlock systems were found working properly during Phase 2.

The SVD had been combined with the PXD, and the VXD has been installed to the Belle II detector already. The Belle II experiment with all the sub-detectors installed will start in March 2019.

Acknowledgments

This work is supported by MEXT, WPI, and JSPS (Japan); ARC (Australia); BMWFW (Austria); MSMT (Czechia); AIDA-2020 (Germany); DAE and DST (India); INFN (Italy); NRF-2016K1A3A7A09005605 and RSRI (Korea); and MNiSW (Poland).

References

[1] E. Kou, P. Urquijo *et al*., arXiv:1808.10567 [hep-ex].

[2] "SuperKEKB," `http://www-superkekb.kek.jp/`

[3] T. Abe *et al*., arXiv:1011.0352 [hep-ex].

[4] M. French *et al*., Nucl. Instrum. Meth. A **466**, 359 (2001).

[5] T. Higuchi *et al*., IEEE Trans. Nucl. Sci. **52**, 1912 (2005).

[6] K. Adamczyk *et al*. [Belle-II SVD Collaboration], Nucl. Instrum. Meth. A **845**, 38 (2017).